Dynamic Spin Fluctuations at $T\rightarrow 0$ in a Spin-1/2 Ferromagnetic Kagome Lattice

Article · November 2013

Source: arXiv

7 authors, including:

Oren Ofer

Technion - Israel Institute of Technology

45 PUBLICATIONS **339** CITATIONS

SEE PROFILE

V Ravi Chandra

National Institute of Science Education and …

16 PUBLICATIONS **81** CITATIONS

SEE PROFILE

Snir Gazit

Technion - Israel Institute of Technology

17 PUBLICATIONS **238** CITATIONS

SEE PROFILE

Daniel Podolsky

Technion - Israel Institute of Technology

56 PUBLICATIONS **1,054** CITATIONS

SEE PROFILE

Dynamic Spin Fluctuations at $T \to 0$ in a Spin-$\frac{1}{2}$ Ferromagnetic Kagomé Lattice

Oren Ofer,[1] Lital Marcipar,[2] V. Ravi Chandra,[3] Snir Gazit,[2] Daniel Podolsky,[2] Daniel P. Arovas,[4] and Amit Keren[2]

[1] *Schulich faculty of Chemistry, Technion - Israel Institute of Technology, Haifa 32000, Israel**
[2] *Department of Physics, Technion - Israel Institute of Technology, Haifa 32000, Israel*
[3] *School of Physical Sciences, National Institute of Science Education and Research, Institute of Physics Campus, Bhbaneswar, 751005 India*
[4] *Department of Physics, University of California at San Diego, La Jolla, California 92093, USA*

(Dated: December 2, 2013)

We report magnetization, electron spin resonance (ESR), and muon spin relaxation (μSR) measurements on single crystals of the $S = 1/2$ (Cu^{+2}) kagomé compound Cu(1,3-benzendicarboxylate). The μSR is carried to temperatures as low as 45 mK. The spin Hamiltonian parameters are determined from the analysis of the magnetization and ESR data. We find that this compound has anisotropic ferromagnetic interactions. Nevertheless, no spin freezing is observed even at temperatures two orders of magnitude lower than the coupling constants. In light of this finding, the relation between persistent spin dynamics and spin liquid are reexamined.

The search for different kinds of quantum spin liquids (SLs) continues to draw considerable experimental attention, and new candidate SLs are reported from time to time [1–9]. Much of the search is focused on compounds with a kagomé lattice. SL lack long range order and are classified according to the presence or absence of a gap to magnetic excitations. The gapless ones, or those with gap smaller than the lowest experimentally available temperature, are expected to have persistent spin dynamics (PSD) at $T \to 0$. A major experimental tool in the search for such states is the muon spin relaxation (μSR) technique. μSR is ideal for this task since it operates at zero external field, without affecting the rotation symmetry of the Hamiltonian. In addition, it can detect the presence or absence of long range order, and dynamic fluctuations. Therefore, PSD has been frequently used to identify materials as SL. However, μSR detected PSD in some compounds that are not expected to be SL such as: pyrochlores [10], molecular magnets [11], and other low dimensional systems [12]. This observation raises a question: can μSR give a false-positive observation when used to identify a SL?

To address this question we investigate the organometallic hybrid kagomé compound Cu(1,3-benzendicarboxylate) [Cu(1,3-bdc)], which was pointed out to be a ferromagnet (FM) at low temperatures [13]. Cu(1,3-bdc), with the chemical formula $CuC_8H_4O_4$, has the ideal qualities of a spin-1/2 kagomé featuring a non-magnetic 1,3-bdc ligand which links the Cu^{+2} kagomé layers [13]. Initial magnetization measurements on polycrystalline samples of Cu(1,3-bdc) suggested that the mean nearest-neighbor super-exchange interaction is antiferromagnetic (AFM) in nature with a Curie-Weiss (CW) temperature of $\Theta_{CW} = -33$ K, yet at low temperatures the onset of a FM signal was observed [13]. Ferromagnetic correlation on a kagomé lattice means that the degree of frustration is low, and therefore the spins should freeze at low temperatures. Nevertheless, early μSR measurements showed only slowing down of the spin fluctuations below $T_s = 1.8$ K. The measurements were carried out only down to 0.9 K, where the magnetic state remains dynamic with no long range order [14].

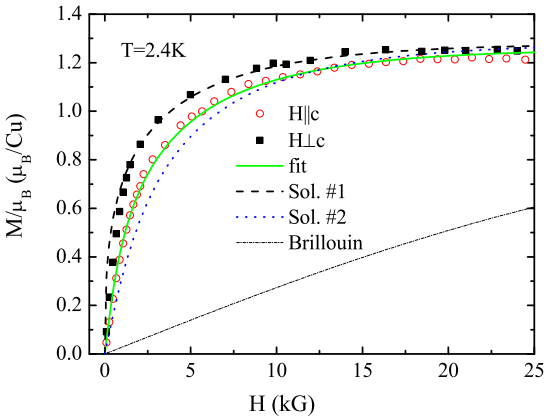

FIG. 1. (Color online) Magnetization of Cu(1,3-bdc) at $T = 2.4$ K, measured at two directions of the crystal: $\mathbf{H} \| \hat{\mathbf{c}}$ (black filled symbols) and $\mathbf{H} \perp \hat{\mathbf{c}}$ (red hollow symbols). The dashed-dotted line indicates a spin-1/2 Brillouin function with $g = 2.0023$. The solid line indicates a fit to a Brillouin function with an effective field (see Eq. 2). The dashed (dotted) curves show the Brillouin function with an effective field using two possible derived Hamiltonian parameters given in table I.

Recently, single crystals were successfully synthesized in the form of millimeter size flakes. Here we combine direction dependent bulk magnetization and Electron Spin Resonance (ESR) measurements to characterize the spin Hamiltonian of these crystals. We show that Cu(1,3-bdc) is an anisotropic, slightly frustrated, ferromagnet; it is certainly not a SL. We also extend the temperature dependence of the previous μSR measurements and show

* oren@physics.technion.ac.il

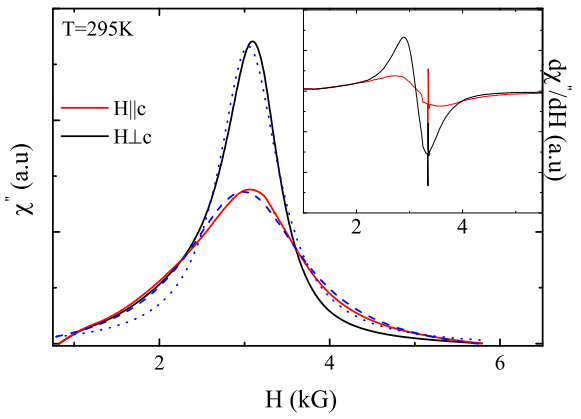

FIG. 2. (Color online) Representative ESR data for the two measured directions, $\mathbf{H}\|\hat{\mathbf{c}}$ (red) and $\mathbf{H}\perp\hat{\mathbf{c}}$ (black), taken at $T = 295$ K. The inset displays the ESR raw signal. The main panel shows the integrated signal (absorption line). The dashed lines demonstrates the fit to a Lorentzian function.

that the dynamic fluctuations persist down to 45 mK. This result indicates that PSD detected by μSR can give a false-positive when used to identify a SL state.

The bulk magnetization (M) measurements were performed using a commercial superconducting quantum interference device (SQUID) at temperatures $3 \le T \le 140$ K with external fields between $0.1 \le H \le 25$ kG applied along and perpendicular to the kagomé planes, i.e., $\mathbf{H} \parallel \hat{\mathbf{c}}$ and $\mathbf{H} \perp \hat{\mathbf{c}}$. The crystals were held onto a small flat glass using epoxy glue with the $\hat{\mathbf{c}}$ direction perpendicular to the glass. The $\hat{\mathbf{c}}$ direction is also perpendicular to the kagomé plane. The crystal's $\hat{\mathbf{a}}$ and $\hat{\mathbf{b}}$ directions are random. To determine the background signal we measured the contribution from an identical glass with the epoxy (not shown). This measurement indicated no temperature dependence and a negligible background contribution compared to the sample signal.

The magnetization measurements versus field at a temperature of $T = 2.4$ K, for two field directions, are plotted in Fig. 1. At fields higher than about 15 kG the magnetization saturates for both directions. For $\mathbf{H} \perp \hat{\mathbf{c}}$, the saturation is reached at a lower field than for $\mathbf{H} \parallel \hat{\mathbf{c}}$. This means that the generated internal fields are strongest when the spins are in the kagomé plane. The saturation value of the magnetization is $1.231(5)\mu_B$. This suggests that the g factor is higher than 2. For a free spin 1/2, the field dependence of the magnetization $\mathbf{M} = g\mu_B \langle \mathbf{S} \rangle$ is given by the Brillouin function. This function is plotted in Fig. 1 by the dashed-dotted line. Clearly the magnetization saturates at lower applied fields than expected for non-interacting spins in both directions. This means that the internal field is larger than the external one and that Cu(1,3-bdc) is a ferromagnet in our experimental conditions.

To take interactions into account we consider a fully anisotropic near-neighbours exchange Hamiltonian

$$\mathcal{H} = \sum_{\langle i,j \rangle} \Big(J\mathbf{S}_i \cdot \mathbf{S}_j + DS_i^z S_j^z + E(S_i^x S_j^x - S_i^y S_j^y) + F\left(\mathbf{S}_i \times \mathbf{S}_j\right)_z \Big) - g\mu_B \sum_i \mathbf{S}_i \cdot \mathbf{H}. \quad (1)$$

where the sum is over near-neighbours bonds, J is the exchange coupling, E and D are the anisotropies, and F represents the $\hat{z}$ component of the Dzyaloshinskii-Moriya (DM) term [15], which is often the biggest [16]. The $\hat{\mathbf{x}}$ direction is along each bond, the $\hat{\mathbf{y}}$ direction is in the kagomé plane perpendicular to each bond, the $\hat{\mathbf{z}}$ direction is perpendicular to the kagomé plane. D, E, and F are believed to be due to spin-orbit couplings. F is a first order and E and D are second order effects. Nevertheless, E and D generate differences in the high temperature magnetization between different directions, which, as we show below, occur in our system. Therefore, E and D are certainly part of the Hamiltonian [17]. We start our analysis by assuming $F = 0$, and, as we shell see, there will be no reason to relax this assumption.

In the mean field approximation, the magnetization on each of the three kagomé sublattices d is determined by the effective field this sublattice experiences $\mathbf{H}^d_{\text{eff}}$. This field is due to the external field and the internal field generated by the moments $\mathbf{M}^d$ of the other sublattices, and is given by the generalized Brillouin function

$$\mathbf{M}^d = \frac{g_{\hat{\mathbf{H}}}\mu_B}{2} \tanh\left(\frac{g_{\hat{\mathbf{H}}}\mu_B}{2K_BT} \left|\mathbf{H}^d_{\text{eff}}\right| \right) \hat{\mathbf{H}}^d_{\text{eff}} \quad (2)$$

where $g_{\hat{\mathbf{H}}}$ represents the direction-dependent g-factor. When the external field is in the $\hat{\mathbf{z}}$ direction, all sublattices are magnetized in that direction only, their moments are equal, and

$$\mathbf{H}_{\text{eff}} = [H - z(J+D)M_z/(g\mu_B)^2]\hat{\mathbf{z}} \quad (3)$$

regardless of d; z is the number of neighbors. A solution of the implicit Eqs. 2 and 3 generates $M_z(H, J, D, g_\|)$. We fit this M_z to the $\mathbf{H} \parallel \hat{\mathbf{c}}$ data and find that

$$J + D = -2.04(2)\ K \quad (4)$$

and $g_\| = 2.51(1)$. The fit is plotted in Fig. 1 by the solid line. The calculated magnetization with interactions describes the data quite well. This calculation demonstrates that the interactions in the $\hat{\mathbf{z}}$ direction must be ferromagnetic on order of 1 K.

Other Hamiltonian parameters are obtained from ESR. The ESR measurement were done in the X-band ($\omega_0 = 9.5$ GHz) at $15 \le T \le 300$ K. The applied field was swept between $0.9 \le H \le 6$ kG. The inset in Fig. 2 plots a representative raw ESR data taken at $T = 295$ K of the sample with a DPPH reference. To obtain the absorption line, we subtract the reference signal, and integrate the raw ESR signal over the applied field. The main panel of

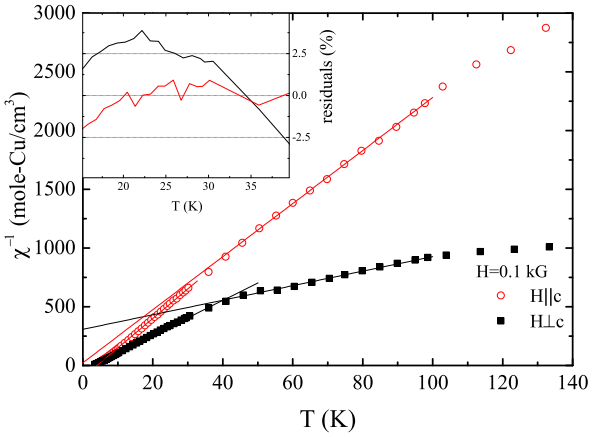

FIG. 3. (Color online) The temperature dependence of the inverse susceptibility $\chi^{-1}(T)$, measured at two directions: $\mathbf{H}\|\hat{\mathbf{c}}$ (filled symbols) and $\mathbf{H}\perp\hat{\mathbf{c}}$ (hollow symbols), the solid lines are fits to a the inverse Curie-Weiss law. The inset shows the residuals from the fit at low temperatures.

Fig. 2 shows the absorption lines for the two measured directions. A reasonable fit to the absorption line is found to a Lorenzian function,

$$\chi''(H) = \frac{A_{\|,\perp}}{\pi}\frac{\delta}{\delta^2 + (H - H_{\|,\perp})^2} \tag{5}$$

where 2δ is the full width-half maximum and $H_{\|,\perp} = \omega_0/(g_{\|,\perp}\mu_B)$ is the resonance field. We find that $g_\perp = 2.164(2)$ and $g_{||} = 2.181(2)$, $\delta_\perp = 0.432(1)$ kG and $\delta_{||} = 0.867(22)$ kG. The δ and g-factor do not have temperature dependence down to 15 K. The area A of the $\mathbf{H}\perp\hat{\mathbf{c}}$ measurement is highest, consistent with the magnetization data, and increases upon cooling as expected. The ESR $g_{\|,\perp}$ factors are larger than 2 but lower than the value determined by the magnetization measurement. The cause of the discrepancy between the magnetization and ESR g factors is not clear to us.

At temperature higher than typical interaction strength, the widths $\delta_{||}$ and $\delta_\perp$ are related to the three Hamiltonian parameters via the moments according to

$$g_{\|,\perp}\mu_B\delta_{\|,\perp} = \frac{\pi}{\sqrt{3}}M_2^{\|,\perp}\sqrt{\frac{M_2^{\|,\perp}}{M_4^{\|,\perp}}}, \tag{6}$$

where $M_2^{\|,\perp} = -Tr\left([\mathcal{H}, S_{\perp,\|}]^2\right)/Tr\left(S_{\perp,\|}{}^2\right)$ and $M_4^{\|,\perp} = Tr\left([\mathcal{H},[\mathcal{H}, S_{\perp,\|}]]^2\right)/Tr\left(S_{\perp,\|}{}^2\right)$ are the second and fourth moments respectively, and $S_{\perp,\|}$ stands for the spin component perpendicular or parallel to the applied field respectively. For the Hamiltonian of Eq. 1, on a kagomé lattice, and for each of the field orientation, we obtain the second and fourth moments as given in the supplementary material. When taking $F = 0$ the second

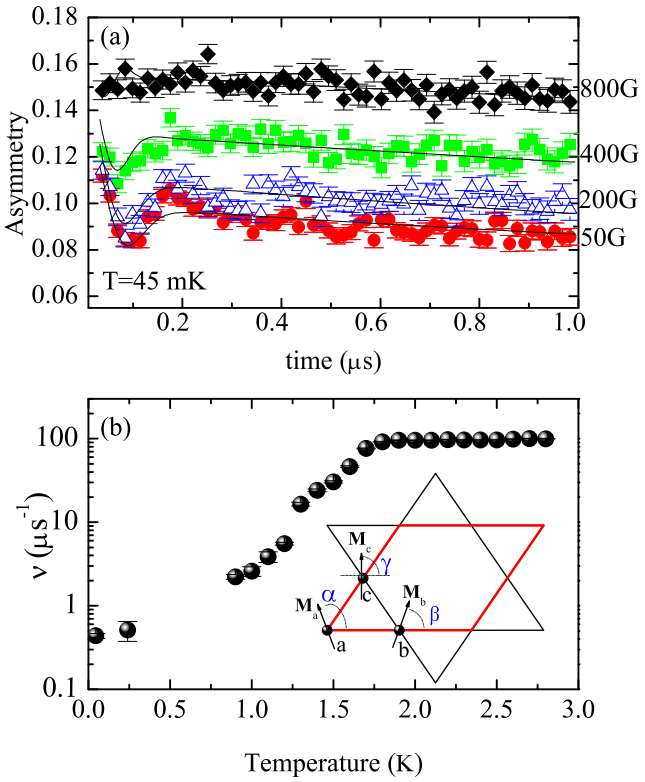

FIG. 4. (Color online) (a) The raw μSR data with applied longitudinal field of 50 to 800 G, the solid lines demonstrate the fit to Eq. 11. (b) A semi-log scale of the spins fluctuation rate ν obtained in Ref. [14] with the added points at 240 mK and 45 mK. Inset: the kagome unit cell (bold red) with its three sublatices (a,b and c) the corresponding magnetic moment ($\mathbf{M}^a$, $\mathbf{M}^b$ and $\mathbf{M}^c$) and angles (α, β, γ).

moments are given by

$$M_2^\perp = 4E^2 \tag{7}$$

$$M_2^{||} = E^2 + D^2, \tag{8}$$

and the fourth moments up to second order in anisotropies are given by

$$M_4^\perp = 18J^2E^2 \tag{9}$$

$$M_4^{||} = \frac{9}{2}J^2E^2 + 3J^2D^2 \tag{10}$$

We numerically solve Eqs. 6 and 4. All the possible solutions of these equations are given in Table I. In both solutions $J + D < 0$ and $J \pm E < 0$ and, as stated above, the interactions between spins are ferromagnetic in all directions.

To check our conclusion, and to verify the assumption made so far, we use the calculated Hamiltonian param-

Sol. #	J (K)	D (K)	E (K)
1	-2.3822	0.3421	± 0.14217
2	-1.7470	-0.2930	± 0.12175

TABLE I. The Hamiltonian parameters derived from the solution of Eq. 6 and 4.

eters to generate the expected field dependent magnetization in the perpendicular direction $\langle M_\perp \rangle (H, J, E, g_\perp)$ and compare it to the data in Fig. 1. For this purpose we calculate the two component magnetization of each of the three kagomé sublattices $\mathbf{M}^d$ for $\mathbf{H} \perp \hat{\mathbf{c}}$, by solving the six coupled explicit Eqs. 2. The $\mathbf{H}^d_{\text{eff}}$ expressions are given in the supplementary material. We then average the magnetization on the three sublattices and project the result onto the $\hat{\mathbf{H}}$ direction to generate $\langle M_\perp \rangle$ as measured experimentally. For all applied field values, the result is independent of the applied field direction in the plane. The g-factor determined from the high field data is $g_\perp = 2.55(4)$. In Fig. 1 we show the calculated $\langle M_\perp \rangle$ for the two possible sets of parameters from Table I. Only solution 1 in the table agrees with the data. The agreement with the data is nearly prefect. Therefore, one can fit all our data without the need to introduce F.

We attempt to confirm these results by temperature dependent susceptibility $\chi \equiv M/H$ measurements for $H \to 0$. The inverse susceptibility χ^{-1} as a function of temperature, for both field orientations with an applied field of 0.1 kG, is depicted in Fig. 3. χ^{-1} is clearly different between the two directions. We performed a high temperature fit to the inverse Curie-Weiss (CW) law, $\chi(T)^{-1} = (T - \Theta_{\text{CW}})/C$, where C is the Curie constant, and Θ_{CW} is the CW temperature. For the two experiments the fit was applied in two temperature ranges: low-T [5 K, 30 K] and high-T [50 K, 100 K]. Above 100 K $\chi(T)^{-1}$ is no longer linear with T for both directions. The CW temperature for $\mathbf{H} \parallel \hat{\mathbf{c}}$ from the high-T range is $-1.0(8)$ K, and from the low-T range is $\Theta^{||}_{\text{CW}} = 4.03$ K. The CW temperature for $\mathbf{H} \perp \hat{c}$ from the high-T is $\Theta^{\perp}_{\text{CW}} = -49(2)$ K. For low-T, $\mathbf{H} \perp \hat{c}$, the data is not linear and could not be fitted reliably. The inset of Fig. 3 displays the difference between the fitted curve and the experimental data. It is clear that above ≈ 15 K, this difference for $(\chi(T)^{\perp})^{-1}$ deviates greatly from 0, whereas the difference for $(\chi(T)^{\parallel})^{-1}$ is close to 0. This type of analysis provides a reliable Θ_{CW} only when the temperature range used in the fit is much larger than the CW temperature obtained by the fit. For $\mathbf{H} \perp \hat{\mathbf{c}}$ this condition is not obeyed in the high temperature range. Therefore $\Theta^{\perp}_{\text{CW}}$ is ambiguous. For $\mathbf{H} \parallel \hat{c}$ both temperature ranges are valid, but give conflicting values of $\Theta^{||}_{\text{CW}}$.

The situation is even more confusing when analyzing the Curie constant for the different directions and temperature ranges. We found that in both temperature ranges, the Curie constant is substantially different between the different directions, and much smaller than expected from localized spin 1/2 on each Cu site. We therefore abandon susceptibility measurements as a mean of characterizing the Hamiltonian.

We now turn to discuss the longitudinal fields (LF) μSR results. The data were collected at the M15 surface muon beamline at TRIUMF using a dilution refrigerator spectrometer. The spectra were gathered at $T = 45$ mK and $T = 240$ mK. In the LF-mode the external field is applied along the initial muon spin direction. When the internal fields fluctuate in space and time, the muon spin polarization is expected to complete less than one full oscillation, and then to relax. The frequency of oscillation increases and the relaxation rate decreases as the field increases. This behavior is described by the dynamical LF Kubo-Toyabe (DLFKT) function $G(\Delta, \nu, t, H_{\text{LF}})$, where ν is the field fluctuation rate, Δ is the static width of the local field distribution, and H_{LF} is the applied field [18].

Figure 4(a) shows the spectra obtained with different fields at $T = 45$ mK. The data exhibits a typical DLFKT behavior in every respect. We fit the function

$$A(t) = A_0 G(\Delta, \nu, t, H_{\text{LF}}) + B_g \tag{11}$$

to the data where $A(t)$ is the muon asymmetry, and B_g is a non-relaxing background due to muons stopping in the sample holder. All the fit parameters are shared for all the data sets at a given temperature. The instantaneous internal field distribution is assumed to be Gaussian. The fit is demonstrated by the solid lines in Fig 4(a). We obtain that $\nu = 0.43(2)\mu\text{s}^{-1}$ and $\Delta = 19.3450(4)$ MHz. The value for Δ is consistent with previous measurements [14] indicating the same field distribution from the millikelvin to few Kelvin range. In contrast, ν decreases by a factor of ≈ 8 relative to data obtained before at a temperature 20 times larger (0.9 K) [14]. We add the new ν values to the previous results in Fig. 4(b). The full picture clearly shows dramatic slowing of the spin fluctuations below ≈ 1.8 K. However the system continues to fluctuate even at 0.05 K with no signs of freezing. Between 240 mK and 45 mK ν is finite, clearly measurable by μSR, and temperature independent.

It should be pointed out that the analysis of the μSR data was done assuming that the muon experiences only the external field. However, in a ferromagnet the internal field is larger than the external field. Unfortunately, without proper knowledge of the muon stopping site it is difficult to estimate the internal field. Analysis of the our data with a field larger than H_{LF} could only lead to higher values of ν. Therefore, the ν in Fig. 4(b) should be considered as lower limit on the real values.

Finite fluctuation rate ν at $T \to 0$, with different time scales, was observed in many kagomé lattices with antiferromagnetic interactions such as SCGO [1], Volborthite [2, 3], Herbertsmithite [4, 5], $Nd_3Ga_5SiO_{14}$[6], Langasite [7], Kapellasite [8], and vanadium-oxyfluoride [9]. All these compounds are considered to be SL. However the Hamiltonian in Eq. 1, with the parameters in Table I, gives a ground state that is fundamentally different from these spin liquids. Since $D > |E|$ the spin lie in the xy plane. This allows us to define one angle per spin as

shown in the inset of Fig. 4(b). For positive or negative E the spins would like to lie parallel or perpendicular to a bond, respectively. However, the ground state energy minimum is reached when two spins make the angles $\alpha = -\beta = -\sqrt{3}E/(6J - E)$ with a bond, and the third spin has $\gamma = 0$ and is 60 degrees away from a bond (see supplementary material). This is a slightly frustrated spin arrangement. A new energy minimum for all the spins on the lattice is found every 60 degrees, but there is no local continuous degeneracy. The energy minimum is shallow and it takes ~ 10 mK per unit cell to overcome the potential barrier and move the entire spin system collectively between local energy minima. This means that Cu(1,3-bdc) should order magnetically and it is not a spin liquid.

In summary, the Cu(1,3-bdc), with Cu^{+2} spin-1/2 situated on kagomé lattice, exhibits anisotropic but ferromagnetic interactions in all direction. μSR indicates persistent spin dynamics down to 45 mK as expected from a spin liquid. The same behavior was observed in many kagomé lattices with AFM interactions. This is very surprising given that a kagomé lattice with ferromagnetic interactions has very small degree of frustration, lacks continuous local degeneracy, and is not a spin liquid. Therefore, μSR can falsely identify a spin liquid.

This work was supported by the Israel USA binational science foundation. We would like to thank Young S. Lee and Joel S. Helton for providing us with the samples. The authors wishes to thank the TRIUMF staff for help with the μSR experiments. Helpful discussions with Sarah Dunsiger are greatly acknowledged.

I. SUPPLEMENTARY MATERIAL

A. Moments

The evaluation of the linewidths in ESR at high temperatures involves calculating the second and fourth order moments to be used in Eq. 6 in the main text. Thus we need to evaluate the first and second order commutators of the total spin component in a given direction and the Hamiltonian. It is straightforward to see that for a spin-1/2 Hamiltonian the first order commutator gives rise to two-spin terms. The second order commutator gives rise to single spin or three spin terms depending on whether a bond term, from the Hamiltonian, and a two spin term from the first order commutator, share two sites or one.

The evaluation of the traces involves careful bookeeping of all the different terms possible. We accomplished that by writing a Mathematica program which evaluates all the terms that can arise and computes the trace. The program evaluates the moments for a general Hamiltonian of spin-1/2 sites. It is assumed that the lattice can be grouped into clusters of sites, which can be seen as sublattices corresponding to a particular Bravais lattice site. The Hamiltonian is then specified as the sum of interactions within a cluster and between clusters. Thus we assume that the Hamiltonian has translation invariance. The input to the program specifies all the site indices and coupling coefficients (9 in number, for $S_{i\alpha}S_{j\beta}$) for all the different bonds involving spins from the Bravais lattice site at the origin. The rest of the bonds on the lattice and their contributions to the trace can be evaluated given the translation invariance. Thus the evaluation is quite general and can be extended to several other systems with more general Hamiltonians such as those containing all the components of the DM interaction and also longer range exchange interactions.

The moments in this paper have been evaluated for the anisotropic kagomé Hamiltonian with three exchange coupling constants and a Dzyaloshinski-Moriya (DM) term given in Eq. 1 of the main text. They are given by:

$$M_2^{\perp} = 4E^2 \tag{12}$$

$$M_2^{||} = F^2 + E^2 + D^2 \tag{13}$$

$$\begin{aligned} M_4^{\perp} =& 18J^2E^2 + 28E^4 + 10F^2E^2 + 8\sqrt{3}FE^2J \\ &+ 4\sqrt{3}FE^2D + 20JDE^2 + 8E^2D^2 \end{aligned} \tag{14}$$

$$\begin{aligned} M_4^{||} =& \frac{11}{2}F^4 - JDE^2 + \frac{9}{2}J^2E^2 + 3J^2D^2 \\ &+ 2JD^3 - \frac{5\sqrt{3}}{2}FE^2D + \frac{13}{4}E^4 + \frac{5}{2}D^4 \\ &+ \frac{41}{4}F^2E^2 + 2F^2J^2 + 3F^2D^2 + \frac{25}{4}E^2D^2 \end{aligned} \tag{15}$$

B. Effective Fields

The kagomé lattice is constructed from three sublattices. They are presented in Fig. 4(b) of the paper. The effective fields in the three different sublattices are:

$$\begin{aligned} \mathbf{H}^a_{\text{eff}} = \mathbf{H} - \frac{2J}{g^2\mu_B^2}(\mathbf{M}^b + \mathbf{M}^c) - \frac{E}{g^2\mu_B^2}\Big(&2M_x^b \\ &- M_x^c + \sqrt{3}M_y^c, -2M_y^b + M_y^c + \sqrt{3}M_x^c\Big) \end{aligned} \tag{16}$$

$$\begin{aligned} \mathbf{H}^b_{\text{eff}} = \mathbf{H} - \frac{2J}{g^2\mu_B^2}(\mathbf{M}^a + \mathbf{M}^c) - \frac{E}{g^2\mu_B^2}\Big(&2M_x^a \\ &- M_x^c - \sqrt{3}M_y^c, -2M_y^a + M_y^c - \sqrt{3}M_x^c\Big) \end{aligned} \tag{17}$$

$$\begin{aligned} \mathbf{H}^c_{\text{eff}} = \mathbf{H} - \frac{2J}{g^2\mu_B^2}(\mathbf{M}^b + \mathbf{M}^a) - \frac{E}{g^2\mu_B^2}\Big(&- M_x^a \\ &- M_x^b + \sqrt{3}M_y^a - \sqrt{3}M_y^b, M_y^a + M_y^b + \sqrt{3}M_x^a - \sqrt{3}M_x^b\Big) \end{aligned} \tag{18}$$

C. Ground state

We determine the ground state in the mean field approximation by writing

$$\mathbf{M}^a = M(\cos\alpha, \sin\alpha) \tag{19}$$
$$\mathbf{M}^b = M(\cos\beta, \sin\beta) \tag{20}$$
$$\mathbf{M}^c = M(\cos\gamma, \sin\gamma). \tag{21}$$

The Hamiltonian per unit cell $H = -\frac{1}{2}\left(\mathbf{M}^a \cdot \mathbf{H}^a_{eff} + \mathbf{M}^b \cdot \mathbf{H}^b_{eff} + \mathbf{M}^c \cdot \mathbf{H}^c_{eff}\right)$ in zero external field it is given by

$$\begin{aligned} H = \frac{M^2}{2(g\mu_B)^2}\{&J\left[4\cos(\alpha-\beta) + 4\cos(\beta-\gamma) + 4\cos(\gamma-\alpha)\right] + \\ &E[4\cos(\alpha+\beta) + 2\sqrt{3}\sin(\alpha+\gamma) - 2\sqrt{3}\sin(\beta+\gamma) \\ &-2\cos(\alpha+\gamma) - 2\cos(\beta+\gamma)]\} \end{aligned} \tag{22}$$

This Hamiltonian is invariant under rotations by 120 degrees and cyclic permutations of the angles. A numerical search for the minimum shows that it occurs at $\alpha = -\beta$, and $\gamma = 0$. Given these relations, and that for each sublattice $\mathbf{H}^d_{\text{eff}}$ is parallel to $\mathbf{M}^d$, we find that $\alpha = -\beta = -\sqrt{3}E/(6J - E)$.

[1] Y. J. Uemura, A. Keren, K. Kojima, L. P. Le, G. M. Luke, W. D. Wu, Y. Ajiro, T. Asano, Y. Kuriyama, M. Mekata, H. Kikuchi, and K. Kakurai, Phys. Rev. Lett. **73** 3306 (1994).

[2] A. Fukaya, Y. Fudamoto, I. M. Gat, T. Ito, M. I. Larkin, A. T. Savici, Y. J. Uemura, P. P. Kyriakou, G. M. Luke, M. T. Rovers, K. M. Kojima, A. Keren, M. Hanawa, and Z. Hiroi, Phys. Rev. Lett. **91**, 207603 (2003)

[3] F. Bert, D. Bono, P. Mendels, J-C. Trombe, P. Millet, A. Amato, C. Baines, and A. Hillier, J. Phys.: Condens. Matter **16** S829 (2004).

[4] P. Mendels, F. Bert, M. A. de Vries, A. Olariu, A. Harrison, F. Duc, J. C. Trombe, J. S. Lord, A. Amato, and C. Baines, Phys. Rev. Lett. **98**, 077204 (2007).

[5] Oren Ofer and Amit Keren, E. A. Nytko, M. P. Shores, B. M. Bartlett, D. G. Nocera, C. Bains and A. Amato, unpublished arXiv:cont-mat/0610540v2 (2006).

[6] A. Zorko, F. Bert, P. Mendels, P. Bordet, P. Lejay, and J. Robert, Phys. Rev. Lett. **100**, 147201 (2008).

[7] A. Zorko, F. Bert, P. Mendels, P. Bordet, P. Lejay, and J. Robert, Phys. Rev. Lett. **100**, 057202 (2008).

[8] B. Fåk, E. Kermarrec, L. Messio, B. Bernu, C. Lhuillier, F. Bert, P. Mendels,5, B. Koteswararao, F. Bouquet, J. Ollivier, A. D. Hillier, A. Amato, R. H. Colman, and A. S. Wills, Phys. Rev. Lett. **109**, 037208 (2012).

[9] L. Clark, J. C. Orain, F. Bert, M. A. de Vries, F. H. Adidoudi, R. E. Morris P. Lightfoot, J. S. Lord, M. T. F. Telling, P. Bonville, J. P. Attfield, P. Mendels, and A. Harrison, Phys. Rev. Lett. **110**, 207208 (2013).

[10] P. Dalmas de Reotier, A. Yaouanc, L. Keller, A. Cervellino, B. Roessli, C. Bains, A. Forget, C. Vaju, P. C. M. Gubbens, A. Amato, and P. J. C. King, Phys. Rev. Lett. **96** 127202 (2006).; A. Yaouanc, P. Dalmas de Reotier, P. Bonville, J. A. Hodges, V. Glazkov, L. Keller, V. Silkolenko, M. Bartkowiak, A. Amato, C. Bains, P. J. C. King, P. C. M. Gubbens, and A. Forget, Phys. Rev. Lett. **110**, 127207 (2013).; J. S. Gardner, S. R. Dunsiger, B. D. Gaulin, M. J. P. Gingras, J. E. Greedan, R. F. Kiefl, M. D. Lumsden, W. A. MacFarlane, N. P. Raju, J. E. Sonier, I. Swainson, and Z. Tun, Phys. Rev. Lett. **82** 1012 (1999).; A. Keren, J. Gardner, G. Ehlers, A. Fukaya, E. Segal, and Y. Uemura, Phys. Rev. Lett. **92**, 107204 (2004).;

[11] Zaher Salman, Amit Keren, Philippe Mendels, Valerie Marvaud, Ariane Scuiller, Michel Verdaguer, James S. Lord, and Chris Baines, Phys. Rev. B 65, 132403 (2002).

[12] F. L. Pratt, P. J. Baker, S. J. Blundell, T. Lancaster, S. Ohira-Kawamura, C. Baines, Y. Shimizu, K. Kanoda, I. Watanabe and G. Saito, Nature **471**, 612 (2011).

[13] Emily A. Nytko, Joel S. Helton, Peter Muller and D. G. Nocera, J. Am. Chem. Soc. **130**, 2922 (2008).

[14] Lital Marcipar, Oren Ofer, Amit Keren, Emily A. Nytko, Daniel G. Nocera, Young S. Lee, Joel S. Helton, Chris Bains, Phys. Rev. B. 80, 132402 (2009).

[15] M. Elhahal, B. Canals, and C. Lacroix, Phys. Rev. B **66**, 014422 (2002).

[16] A. Zorko, S. Nellutla, J. van Tol, L. C. Brunel, F. Bert, F. Duc, J.-C. Trombe, M. A. de Vries, A. Harrison, and P. Mendels, Phys. Rev. Lett. **101**, 026405 (2008).

[17] Oren Ofer and Amit Keren, Phys. Rev. B **79**, 134424 (2009).

[18] R. S. Hayano, Y. J. Uemura, J. Imazato, N. Nishida, T. Yamazaki, and R. Kubo, Phys. Rev. B **20**, 850 (1979).